metals

MDPI

Communication

Effect of Hydrogen Charging on Pop-in Behavior of a Zr-Based Metallic Glass

Lin Tian [1,2,*], Dominik Tönnies [1], Moritz Hirsbrunner [1], Tim Sievert [1], Zhiwei Shan [2] and Cynthia A. Volkert [1,*]

[1] Institute of Materials Physics, University of Göttingen, 37077 Göttingen, Germany; dominik.toennies@phys.uni-goettingen.de (D.T.); moritz.hirsbrunner@stud.uni-goettingen.de (M.H.); tim.sievert@stud.uni-goettingen.de (T.S.)

[2] Center for Advancing Materials Performance from the Nanoscale (CAMP-Nano) & Hysitron Applied Research Center in China (HARCC), State Key Laboratory for Mechanical Behavior of Materials, Xi'an Jiaotong University, Xi'an 710049, China; zwshan@mail.xjtu.edu.cn

* Correspondence: ltian@phys.uni-goettingen.de (L.T.); volkert@ump.gwdg.de (C.A.V.); Tel.: +49-551-39-25002 (L.T. & C.A.V.)

Received: 12 November 2019; Accepted: 18 December 2019; Published: 22 December 2019

Abstract: In this work, structural and mechanical properties of hydrogen-charged metallic glass are studied to evaluate the effect of hydrogen on early plasticity. Hydrogen is introduced into samples of a Zr-based (Vit 105) metallic glass using electrochemical charging. Nanoindentation tests reveal a clear increase in modulus and hardness as well as in the load of the first pop-in with increasing hydrogen content. At the same time, the probability of a pop-in occurring decreases, indicating that hydrogen hinders the onset of plastic instabilities while allowing local homogeneous deformation. The hydrogen-induced stiffening and hardening is rationalized by hydrogen stabilization of shear transformation zones (STZs) in the amorphous structure, while the improved ductility is attributed to the change in the spatial correlation of the STZs.

Keywords: metallic glass; hydrogen; indentation; pop-in; plasticity

1. Introduction

Metallic glasses (MGs) or amorphous metals are materials composed of metal components but without crystalline structure [1]. In addition to applications as high-performance structural materials [2], the unique structure of MGs makes them promising candidate materials in many other fields. As one of the important applications, MGs can be used as storage and separation media for hydrogen gas (H_2), which is a well-known clean energy source. Zr-based MGs for instance have been observed to absorb large amounts of hydrogen [3] with a content even comparable to the best crystalline hydrogen-storage materials [4] due to their large number of interstitial-like sites and favorable hydrogen–metal chemistry. The high solubility and moderate diffusivity of hydrogen [5] in the amorphous structure also increases H_2 permeability in MGs [6,7]. With high H_2 permeability, high strength, and corrosion resistance, MG films can be used as H_2 separation membranes in hydrogen selective devices [6,8]. As a critical part of the device, MGs must survive mechanical pressure in the gaseous H_2 environment. The performance and stability of MGs in H_2 have significant impact on device safety, and therefore the effects of hydrogen on the mechanical properties of MGs have received increasing attention.

Although the effect of hydrogen in MGs has been studied by several groups in recent years, debates remain on questions such as whether hydrogen is a detrimental [7] or beneficial [9,10] element for MGs, or whether doping hydrogen increases [11] or decreases [12] the strength of MGs. Like in crystalline materials, hydrogen can induce embrittlement in MGs [7,13–15]. In contrast, positive

effects of hydrogen on plasticity have also been found in some alloys. For instance, in Zr-based MGs [9,16–18] which have large negative enthalpies of mixing with hydrogen [19], the hydrogen addition increases both glass-forming ability and ductility, opening a new approach to make both stable and ductile MGs. It has been proposed that hydrogen addition in MGs can introduce local structural heterogeneities which prevent single, catastrophic shear bands and promote the formation of multiple shear bands [16,18,20]. A recent work on elastic heterogeneity actually shows that the spatial correlation of the heterogeneities plays an important role in tuning ductility of MGs [21]. Since hydrogen addition is potentially useful in MG alloy design, the underlying mechanisms of how hydrogen addition improves ductility and stability of MGs deserve further investigation.

In this work, the effect of solid-solution hydrogen on pop-in behavior of an MG is studied. A pop-in during spherical indentation results from an abrupt shear event along a shear band trajectory [22] which represents early plasticity and is a smaller version of the shear bands observed in bulk MGs [22,23]. The results are interpreted in terms of the hydrogen-induced changes to the MG structure and potential energy landscape, and we discuss how hydrogen can be used to control shear band formation. A Zr-based MG of similar composition to those used in several studies in the literature [17,24] is used.

2. Materials and Methods

A Zr-based Vit 105 MG ($Zr_{52.5}Cu_{17.9}Ni_{14.6}Al_{10}Ti_5$) plate with a thickness of 2 mm was produced by suction casting into a Cu-mold. The as-cast samples were cut into thin samples by electrical discharge machining. On each of the samples, the as-cut surface was mechanically polished while the as-cast surface was kept intact for indentation tests. The final sample had an area of ~15 mm^2 and a thickness of 1 mm.

In contrast to previous studies [11], where hydrogen was added to the alloy by processing the melt in a H_2-containing gas, hydrogen charging of samples was performed after quenching using a cathodic charging technique in a 0.5 mol/L sulfuric acid solution. The samples were charged at a current density ~10 mA/cm^2 (lower than the critical current density for the formation of hydride [25]) for various charging times in order to control the dissolved hydrogen content (c_H). Hydrogen contents up to $c_H > 0.5$ H/M (hydrogen-to-metal ratio) were investigated, with most studies focusing on $c_H \leq 0.29$ H/M where no specimen cracking was observed. The structure of the samples before and after hydrogen charging was investigated with X-ray diffraction (Cu-Kα line).

Nanoindentation tests were conducted at room temperature using a Nano Indenter G200 (formerly MTS; now KLA-Tencor, Milpitas, CA, USA). Indentation with a Berkovich indenter in the standard XP indentation head was performed on the samples to measure hardness H and Young's modulus E using the continuous stiffness measurement technique [26]. Reduced Young's modulus E_r is calculated using the slope of the unloading curve and precalibrated contact area of the indenter. The modulus of the sample E_s can be derived from the equation:

$$1/E_r = \left(1-\nu_i^2\right)/E_i + \left(1-\nu_s^2\right)/E_s, \quad (1)$$

where Young's modulus of the tip E_i = 1140 GPa. Poisson's ratios of the diamond tip and the sample are $\nu_i^2 = 0.07$ and $\nu_s^2 = 0.37$, respectively. The indentation depth reaches 2 μm in order to reduce the effect of surface roughness.

A spherical diamond tip with a diameter of R = 650 nm was used in the DCM-1 indenter head. The tip radius was calibrated on a fused silica reference sample. Arrays of 12 × 12 indents which covered an area of 33 × 33 μm^2 were measured with a constant loading rate of 0.1 mN/s to a maximum load of 1 mN corresponding to a displacement of ~50 nm. Displacement bursts, which are commonly referred to as "pop-ins", were visible in the load-displacement curves and automatically identified from displacement-rate data using a MATLAB script (R2013b, MathWorks, Natick, MA, USA). See details in [27]. In order to measure c_H, the average hydrogen content of the sample, melt extraction was carried out on the samples after indentation tests using a Hydrogen analyzer (G8 Galileo, Bruker, Billerica,

MA, USA). The hydrogen analyzer was calibrated by a commercial standard hydrogen containing sample (501-529, Leco, St Joseph, MI, USA). All the indentation tests and melt extraction analysis were performed within 72 h after the samples were charged with hydrogen.

3. Results

X-ray diffraction spectra were recorded and compared for each sample before and after hydrogen charging. The result of X-ray diffraction only reveals a small shift of the broad maxima characteristic of the nearest neighbor distances. In a sample charged to $c_H > 0.5$ H/M (the highest hydrogen content in this work) the position of the broad maxima is shifted to lower 2θ values by 0.5 degrees relative to the as-cast material (see Figure 1a). The lower diffraction angle indicates that on average the hydrogen-charged sample has larger atomic spacing than the uncharged sample. No evidence of hydride formation was found in the samples.

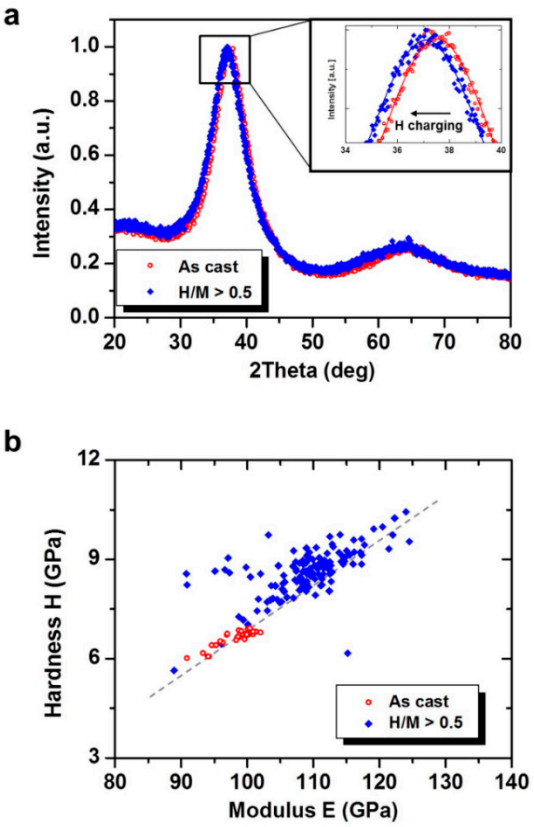

Figure 1. (**a**) X-ray diffraction spectra of Vit 105 metallic glass (MG) samples with and without hydrogen charging. The hydrogen content is defined as the hydrogen-to-metal ratio. (**b**) Hardness and modulus (Berkovich indentation) of samples with and without hydrogen charging. The dashed line is to guide the eye.

Modulus and hardness measured by Berkovich indentation on samples with and without hydrogen charging for $c_H > 0.5$ H/M are plotted in Figure 1b. The average modulus and hardness of the as-cast sample were 98 ± 3 and 6.6 ± 0.2 GPa, respectively. Although there is considerable scatter in the values, both the modulus and the hardness clearly increase as a result of hydrogen charging, leading to average values of 110 ± 7 and 8.7 ± 0.8 GPa, respectively. The modulus and hardness values in both the uncharged and charged states are linearly correlated with each other, suggesting that both properties are determined by the same features of the structure and short-range chemical ordering. Meanwhile, the wider distribution of modulus and hardness values in the charged state indicates larger variations in local structure (more structural heterogeneities) due to hydrogen incorporation on the micrometer

length scale of the Berkovich indents. Some of the data points do not show the linear correlation, in that the modulus is decreased without a significant change in hardness. We attribute this to the formation of surface relaxation or surface cracks which are observed in some regions of the highly charged specimens [28,29].

Mechanical properties of the bulk sample were measured by Berkovich indentation while local plasticity was studied by spherical indentation which is sensitive to early plasticity events in MGs [27]. The first pop-in in the load-displacement curve is attributed to the onset of plasticity and the corresponding maximum shear stress along the shear band trajectory defines the yield stress [22]. Samples were prepared for spherical indentation tests with c_H-values of 0, 0.11, 0.13, and 0.29 H/M. Before indentation tests, the sample surfaces were checked with optical microscopy to make sure there were no cracks. Representative load-displacement curves of indentations from the four different samples are plotted in Figure 2a. Pop-ins can be seen in the data from samples with c_H-values 0, 0.11, and 0.13 H/M. The first pop-in is attributed to the initiation of detectable plasticity [27] and is marked by a solid arrow in each curve. In contrast, the sample with c_H = 0.29 H/M does not show any pop-ins. In order to further analyze the pop-ins, displacement rates were calculated for each curve (Figure 2b) where pop-ins with a displacement larger than a threshold value can be easily identified. Compared to other samples, displacement rate curves for the sample with c_H = 0.29 H/M are very smooth. It is worth noting that there is residual plastic deformation in the indents of the 0.29 H/M sample even though no pop-ins are observed. The data point indicated by the arrow in Figure 2a demonstrates that deformation of the material under the indenter is not fully recoverable. Therefore, the deformation during indentation is already beyond the elastic region but is not able to initiate a pop-in. A statistical evaluation shows that 100% of the indents in the uncharged c_H = 0 H/M sample have pop-ins. This percentage reduces to about 80% in the c_H-value 0.11 and 0.13 H/M samples. In the c_H = 0.29 H/M sample, there are no pop-ins at all in all indentations demonstrating that local homogeneous deformation is occurring. This result is summarized in Figure 2c.

The strength of the sample is evaluated using the maximum shear stress when the first pop-in occurs. Analysis of elastic stress distribution based on Hertzian contact theory [30] reveals that the maximum stress locates underneath the center of the indenter at a depth of half the contact radius [31]. The maximum shear stress is approximated by:

$$\tau_{max} \approx AP_{pop-in}/\left(\pi \times R \times h_{pop-in}\right), \quad (2)$$

with P_{pop-in} and h_{pop-in} being the load and displacement at the onset of the pop-in, respectively, diameter of the spherical diamond tip R = 650 nm, and a pre-factor A = 0.4413 [27]. Cumulative distributions of the maximum shear stresses at the first pop-ins for the c_H-value 0, 0.11, and 0.13 H/M samples are plotted in Figure 3. The pop-in stresses vary by as much as 2 GPa for a given sample, indicating significant structural heterogeneity on a length scale between the size of the indented volume (ca. 1 μm) and the size of the indent array (ca. 35 μm). The average maximum shear stress for uncharged sample 1 is about 2.9 GPa. A clear shift of maximum shear stresses to higher values is shown in hydrogen-charged samples 2 and 3 compared to sample 1. The average maximum shear stress for the charged sample 3 is about 3.2 GPa, 10% higher than that of sample 1. This result showing hydrogen-induced hardening effect is qualitatively consistent with modulus and hardness measurement with Berkovich indentation, as shown in Figure 1b. It can also be noticed that the shape of the distribution curves for samples 2 and 3 is different from that of sample 1. The curve of sample 2 is stretched while the curve of sample 3 is compressed even though they have similar c_H. This difference suggests considerable structural heterogeneity in the hydrogen-charged MG over length scales much larger than the array size of ca. 35 μm. There is no cumulative distribution curve for sample 4 because no pop-ins were observed for any of the 144 indentation tests.

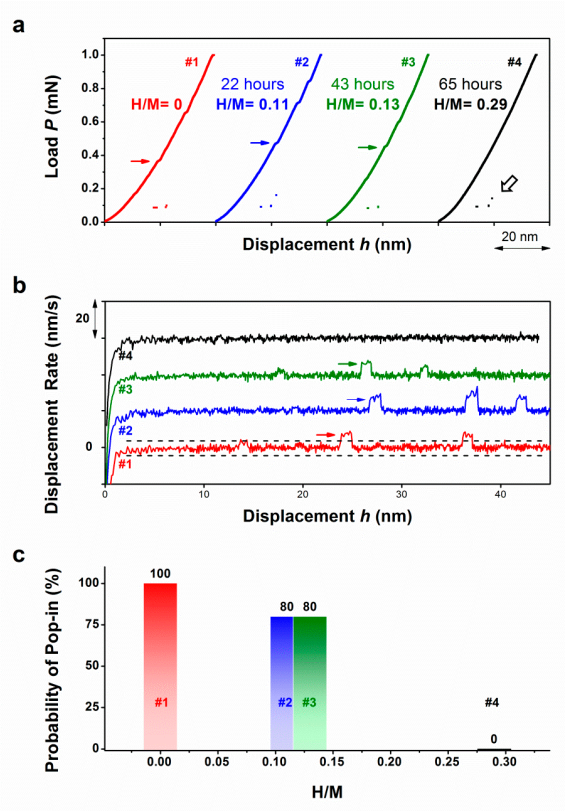

Figure 2. (**a**) Typical load displacement curves for indents in samples with different hydrogen content (c_H). The curves are shifted for the sake of clarity. (**b**) Displacement rate as a function of displacement for each curve in (a). The first pop-ins are marked with arrows. The curves are shifted for the sake of clarity. (**c**) The percentage of indents that have no pop-in out of 144 tests in each sample.

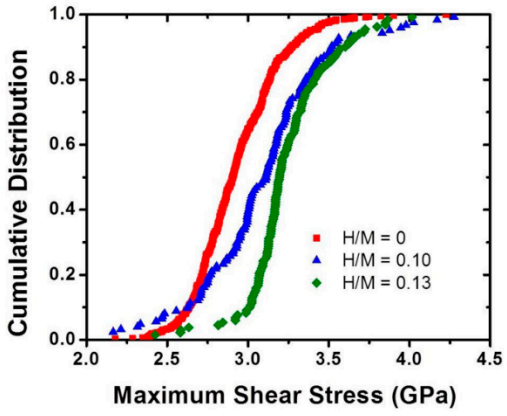

Figure 3. Cumulative distribution of the first pop-ins against the maximum shear stress of samples with different c_H.

4. Discussion

The deformation behavior of MGs is often discussed in terms of a distribution of activation energies for atomic rearrangements [32]. Underlying this distribution of activation energies is the potential energy landscape of the disordered structure [33]. When atomic rearrangements occur, either due to deformation or structural relaxation, they change the glass structure by shifting potential and activation energies. Similarly, hydrogen solid-solution charging of an MG results in local atomic rearrangements and a c_H-dependent increase of the interatomic distances [28,29,34], thereby also

locally shifting potential and activation energies. In the beginning of hydrogen charging, the favored or so-called trapping sites for hydrogen are those with high local potential energies, such as sites with large free volume [35], or geometrically unfavored motifs (GUMs) [36]. Hydrogen also has been found to fill interstitial sites of loosely packed Zr-rich tetrahedral-like sites (t-sites) [3,34,37,38]. These trapping sites are stabilized by the hydrogen [39], lowering the local potential energy and generally resulting in an increase in the local activation energies for atomic rearrangements, thereby restricting deformation [11].

The study here reveals a clear increase in both modulus and hardness due to hydrogen charging. The linear relation between modulus and hardness suggests that the underlying mechanisms controlling stiffness and deformation by atomic rearrangement depend on the same aspects of the atomic structure. A similar correlation between the stiffness and barrier height for local shear rearrangements has been thoroughly investigated and discussed for metallic glass-forming liquids [33]. Furthermore, the fact that the modulus and hardness have the same relation in the uncharged and charged states indicates that the structural changes introduced by hydrogen do not produce fundamentally different mechanical responses than the structural heterogeneities already present in the uncharged disordered structure. The simplest explanation for our observations is that the hydrogen stabilizes regions of low shear modulus, thus increasing the stiffness and hindering atomic rearrangements.

Both increases and decreases of modulus and hardness have been observed in the literature due to hydrogen charging, depending on the alloy composition. MGs with a high Zr composition consistently show increases in mechanical properties on charging, likely because the Zr-rich clusters are made more stable by the inclusion of hydrogen [11,18,40] due to the large negative mixing enthalpy. The incorporation of hydrogen in these clusters presumably makes them more resistant to deformation, increasing the modulus and hardness, as well as the pop-in stress of the MG. On the contrary, hydrogen incorporated into a stable icosahedron cluster may raise the potential energy and make the cluster less stable to atomic rearrangements. As a result, the MG may appear to be softened by hydrogen addition [20].

Beyond the increase in hardness and modulus, the most noticeable effect of hydrogen charging in this study is the replacement of pop-ins by stable or homogeneous flow. The improved ductility and malleability of MGs induced by hydrogen has usually been attributed to an increase in structural heterogeneities in the literature, although an exact mechanism has not been discussed [16,18,20]. There is no doubt that the hydrogen addition changes local environments in the MGs, thereby changing the potential energy distribution which likely accounts for changes in hardness and modulus. In addition to the change in the potential energy distribution, the spatial distribution of sites with different potential energy should be considered. Our recent work suggests an increase of correlation length of medium-range order in a $Zr_{51}Cu_{49}$ MG during hydrogen loading [41]. The spatial correlation of the heterogeneities may play a decisive role in the ductility of MGs. In a simulation study by Wang et al. [21], the mechanical properties of samples with the same potential energy distribution but different correlation lengths for the local shear modulus are compared. To first order, the correlation length simply describes the size and spacing of potential STZs (elastically soft sites) in the MG. Their results reveal that when the correlation length increases from 0.5 to 5 nm, a transition in deformation mechanism from "stress-dictated" shear band nucleation and growth to a "structural-dictated" strain percolation occurs [21]. This is associated with a decrease in the tendency for strain localization and an increase in the plastic strain to failure. The basic understanding of this observation is that more widely spaced STZs cannot easily interact through their stress fields, thus hindering the formation of shear bands through collective excitation. Building on the model of Wang et al., we propose that hydrogen stabilization of STZs decreases their density, thereby increasing the correlation length and hindering strain localization and pop-in instabilities. We further suggest that the high mobility of the hydrogen may allow it to change sites in response to changing strain fields, thus inhibiting propagation of excitations between STZs and hindering pop-in formation. If hydrogen is able to move in response

to strain fields introduced by other hydrogen atoms, some form of self-organization of the hydrogen is expected to be active.

Potential sites that can be filled with hydrogen are limited in MGs since the maximum solubility of hydrogen is low. When the sample is overcharged with hydrogen [28,29], cracks presumably form due to hydrogen-induced expansion and the possible motion of hydrogen in the resultant strain fields. Precise control of c_H will be required when using hydrogen to optimize the mechanical behavior of MGs.

Heterogeneities at various length scales have been discussed here, ranging from the flexibility volumes, free volume defects, STZs, and GUMs at the nanometer scale up to the observed variations in modulus, hardness, and pop-in stresses at the micrometer scale. Whether the hydrogen-induced changes in nanometer scale heterogeneities can result in the observed micrometer-scale variations will depend on the distribution of spatial correlations as well as the ability of hydrogen to move in response to the hydrogen-induced strain fields. Confirmation of the nanometer-scale heterogeneity changes as well as evidence for possible self-organization due to hydrogen charging remain elusive due to technical limitations. However, state-of-the-art methods such as fluctuation electron microscopy [42,43] may open the possibility to track the evolution of nanoscale heterogeneities during hydrogen charging.

5. Conclusions

Our results show a clear effect of hydrogen on the mechanical behavior of a Vit 105 MG. With increasing hydrogen content up to 0.29 H/M, the load of the first pop-in increases, consistent with the observed increase in hardness and modulus, while the occurrence of pop-ins decreases. This results in a transition from pop-in or shear banding to homogeneous deformation at a hydrogen content of 0.29 H/M. The behavior is interpreted in terms of hydrogen stabilization of STZs in the amorphous structure due to the negative enthalpy of mixing of hydrogen with Zr. Thus, charging of MGs with negative heats of mixing with low concentration of hydrogen may offer a robust method to increase modulus and hardness and prevent catastrophic shear band formation in MGs.

Author Contributions: Conceptualization, L.T., D.T. and C.A.V.; Methodology and Formal Analysis, D.T., M.H. and T.S.; Writing—Review and Editing, L.T., D.T. and C.A.V.; Funding Acquisition, L.T., Z.S. and C.A.V. All authors have read and agreed to the published version of the manuscript.

Funding: L.T. acknowledges the Natural Science Foundation of China (Grant 51501144), the China Postdoctoral Science Foundation (2015M580842), and the Alexander von Humboldt Foundation for financial support. C.A.V. and D.T. acknowledge financial support by the German Research Foundation (DFG) through an individual grant (VO 928/9-1). Z.W.S. acknowledges support by the National Key Research and Development Program of China (No. 2017YFB0702001) and Natural Science Foundation of China (51231005 and 51621063).

Acknowledgments: We would also like to thank Feng Jiang and Mingcan Li for providing the samples.

Conflicts of Interest: The authors declare no conflict of interest.

References

1. Klement, W.; Willens, R.H.; Duwez, P. Non-crystalline Structure in Solidified Gold-Silicon Alloys. *Nature* **1960**, *187*, 869–870. [CrossRef]
2. Inoue, A.; Takeuchi, A. Recent Development and Applications of Bulk Glassy Alloys. *Int. J. Appl. Glass Sci.* **2010**, *1*, 273–295. [CrossRef]
3. Bankmann, J.; Pundt, A.; Kirchheim, R. Hydrogen loading behaviour of multi-component amorphous alloys: Model and experiment. *J. Alloys Compd.* **2003**, *356–357*, 566–569. [CrossRef]
4. Zander, D.; Tal-Gutelmacher, E.; Jastrow, L.; Köster, U.; Eliezer, D. Hydrogenation of Pd-coated Zr-Cu-Ni-Al metallic glasses and quasicrystals. *J. Alloys Compd.* **2003**, *356–357*, 654–657. [CrossRef]
5. Wang, Y.I.; Suh, J.Y.; Lee, Y.S.; Shim, J.H.; Fleury, E.; Cho, Y.W.; Koh, S.U. Direct measurement of hydrogen diffusivity through Pd-coated Ni-based amorphous metallic membranes. *J. Membr. Sci.* **2013**, *436*, 195–201. [CrossRef]

6. Yamaura, S.; Sakurai, M.; Hasegawa, M.; Wakoh, K.; Shimpo, Y.; Nishida, M.; Kimura, H.; Matsubara, E.; Inoue, A. Hydrogen permeation and structural features of melt-spun Ni-Nb-Zr amorphous alloys. *Acta Mater.* **2005**, *53*, 3703–3711. [CrossRef]
7. Paglieri, S.N.; Pal, N.K.; Dolan, M.D.; Kim, S.M.; Chien, W.M.; Lamb, J.; Chandra, D.; Hubbard, K.M.; Moore, D.P. Hydrogen permeability, thermal stability and hydrogen embrittlement of Ni-Nb-Zr and Ni-Nb-Ta-Zr amorphous alloy membranes. *J. Membr. Sci.* **2011**, *378*, 42–50. [CrossRef]
8. Dolan, M.D.; Dave, N.C.; Ilyushechkin, A.Y.; Morpeth, L.D.; McLennan, K.G. Composition and operation of hydrogen-selective amorphous alloy membranes. *J. Membr. Sci.* **2006**, *285*, 30–55. [CrossRef]
9. Dong, F.; Su, Y.; Luo, L.; Wang, L.; Wang, S.; Guo, J.; Fu, H. Enhanced plasticity in Zr-based bulk metallic glasses by hydrogen. *Int. J. Hydrog. Energy* **2012**, *37*, 14697–14701. [CrossRef]
10. Su, Y.; Dong, F.; Luo, L.; Guo, J.; Han, B.; Li, Z.; Wang, B.; Fu, H. Bulk metallic glass formation: The positive effect of hydrogen. *J. Non-Cryst. Solids* **2012**, *358*, 2606–2611. [CrossRef]
11. Zhao, Y.; Choi, I.C.; Seok, M.Y.; Kim, M.H.; Kim, D.H.; Ramamurty, U.; Suh, J.Y.; Jang, J.i. Effect of hydrogen on the yielding behavior and shear transformation zone volume in metallic glass ribbons. *Acta Mater.* **2014**, *78*, 213–221. [CrossRef]
12. Dandana, W.; Yousfi, M.; Hajlaoui, K.; Gamaoun, F.; Yavari, A. Thermal stability and hydrogen-induced softening in $Zr_{57}Al_{10}Cu_{15.4}Ni_{12.6}Nb_5$ metallic glass. *J. Non-Cryst. Solids* **2017**, *456*, 138–142. [CrossRef]
13. Schroeder, H.W.; Koster, U. Hydrogen embrittlement of metallic glasses. *J. Non-Cryst. Solids* **1983**, *56*, 213–218. [CrossRef]
14. Lin, J.J.; Perng, T.P. Embrittlement of amorphous $Fe_{40}Ni_{38}Mo_4B_{18}$ alloy by electrolytic hydrogen. *Metall. Mater. Trans. A-Phys. Metall. Mater. Sci.* **1995**, *26*, 197–201. [CrossRef]
15. Jayalakshmi, S.; Fleury, E. Hydrogen embrittlement in metallic amorphous alloys: An overview. *J. ASTM Int.* **2010**, *7*, 1–23.
16. Dong, F.; Lu, S.; Zhang, Y.; Luo, L.; Su, Y.; Wang, B.; Huang, H.; Xiang, Q.; Yuan, X.; Zuo, X. Effect of hydrogen addition on the mechanical properties of a bulk metallic glass. *J. Alloys Compd.* **2017**, *695*, 3183–3190. [CrossRef]
17. Granata, D.; Fischer, E.; Löffler, J.F. Hydrogen microalloying as a viable strategy for enhancing the glass-forming ability of Zr-based bulk metallic glasses. *Scr. Mater.* **2015**, *103*, 53–56. [CrossRef]
18. Granata, D.; Fischer, E.; Löffler, J.F. Effectiveness of hydrogen microalloying in bulk metallic glass design. *Acta Mater.* **2015**, *99*, 415–421. [CrossRef]
19. Yamanaka, S.; Tanaka, T.; Miyake, M. Effect of oxygen on hydrogen solubility in zirconium. *J. Nucl. Mater.* **1989**, *167*, 231–237. [CrossRef]
20. Zhao, Y.; Choi, I.C.; Seok, M.Y.; Ramamurty, U.; Suh, J.Y.; Jang, J.i. Hydrogen-induced hardening and softening of Ni-Nb-Zr amorphous alloys: Dependence on the Zr content. *Scr. Mater.* **2014**, *93*, 56–59. [CrossRef]
21. Wang, N.; Ding, J.; Yan, F.; Asta, M.; Ritchie, R.O.; Li, L. Spatial correlation of elastic heterogeneity tunes the deformation behavior of metallic glasses. *npj Comput. Mater.* **2018**, *4*, 19. [CrossRef]
22. Packard, C.; Schuh, C. Initiation of shear bands near a stress concentration in metallic glass. *Acta Mater.* **2007**, *55*, 5348–5358. [CrossRef]
23. Greer, A.L.; Cheng, Y.Q.; Ma, E. Shear bands in metallic glasses. *Mater. Sci. Eng. R Rep.* **2013**, *74*, 71–132. [CrossRef]
24. Dong, F.; He, M.; Zhang, Y.; Luo, L.; Su, Y.; Wang, B.; Huang, H.; Xiang, Q.; Yuan, X.; Zuo, X.; et al. New insights into melt hydrogenation effects on glass-forming ability in a Zr-based bulk metallic glass. *J. Non-Cryst. Solids* **2018**, *481*, 170–175. [CrossRef]
25. Gostin, P.F.; Eigel, D.; Grell, D.; Uhlemann, M.; Kerscher, E.; Eckert, J.; Gebert, A. Stress-corrosion interactions in Zr-based bulk metallic glasses. *Metals* **2015**, *5*, 1262–1278. [CrossRef]
26. Oliver, W.C.; Pharr, G.M. An improved technique for determining hardness and elastic modulus using load and displacement sensing indentation experiments. *J. Mater. Res.* **1992**, *7*, 1564–1583. [CrossRef]
27. Tönnies, D.; Samwer, K.; Derlet, P.M.; Volkert, C.A.; Maaß, R. Rate-dependent shear-band initiation in a metallic glass. *Appl. Phys. Lett.* **2015**, *106*, 171907. [CrossRef]
28. Ismail, N.; Uhlemann, M.; Gebert, A.; Eckert, J. Hydrogenation and its effect on the crystallisation behaviour of $Zr_{55}Cu_{30}Al_{10}Ni_5$ metallic glass. *J. Alloys Compd.* **2000**, *298*, 146–152. [CrossRef]

29. Jayalakshmi, S.; Fleury, E.; Leey, D.Y.; Chang, H.J.; Kim, D.H. Hydrogenation of $Ti_{50}Zr_{25}Co_{25}$ amorphous ribbons and its effect on their structural and mechanical properties. *Philos. Mag. Lett.* **2008**, *88*, 303–315. [CrossRef]
30. Johnson, K.L. *Contact Mechanics*; Cambridge University Press: Cambridge, UK, 1987.
31. Bei, H.; Lu, Z.; George, E. Theoretical strength and the onset of plasticity in bulk metallic glasses investigated by nanoindentation with a spherical indenter. *Phys. Rev. Lett.* **2004**, *93*, 125504. [CrossRef]
32. Hufnagel, T.C.; Schuh, C.A.; Falk, M.L. Deformation of metallic glasses: Recent developments in theory, simulations, and experiments. *Acta Mater.* **2016**, *109*, 375–393. [CrossRef]
33. Johnson, W.L.; Demetriou, M.D.; Harmon, J.S.; Lind, M.L.; Samwer, K. Rheology and Ultrasonic Properties of Metallic Glass-Forming Liquids: A Potential Energy Landscape Perspective. *MRS Bull.* **2011**, *32*, 644–650. [CrossRef]
34. Samwer, K.; Johnson, W. Structure of glassy early-transition-metal-late-transition-metal hydrides. *Phys. Rev. B* **1983**, *28*, 2907. [CrossRef]
35. Spaepen, F. A microscopic mechanism for steady state inhomogeneous flow in metallic glasses. *Acta Metall.* **1977**, *25*, 407–415. [CrossRef]
36. Ding, J.; Patinet, S.; Falk, M.L.; Cheng, Y.; Ma, E. Soft spots and their structural signature in a metallic glass. *Proc. Natl. Acad. Sci. USA* **2014**, *111*, 14052–14056. [CrossRef] [PubMed]
37. Harris, J.; Curtin, W.; Tenhover, M. Universal features of hydrogen absorption in amorphous transition-metal alloys. *Phys. Rev. B* **1987**, *36*, 5784. [CrossRef]
38. Chuang, A.C.-P.; Liu, Y.; Udovic, T.J.; Liaw, P.K.; Yu, G.-P.; Huang, J.-H. Inelastic neutron scattering study of the hydrogenated $(Zr_{55}Cu_{30}Ni_5Al_{10})_{99}Y_1$ bulk metallic glass. *Phys. Rev. B* **2011**, *83*, 174206. [CrossRef]
39. Suh, D.; Asoka-Kumar, P.; Dauskardt, R.H. The effects of hydrogen on viscoelastic relaxation in Zr-Ti-Ni-Cu-Be bulk metallic glasses: Implications for hydrogen embrittlement. *Acta Mater.* **2002**, *50*, 537–551. [CrossRef]
40. Dong, F.; He, M.; Zhang, Y.; Luo, L.; Su, Y.; Wang, B.; Huang, H.; Xiang, Q.; Yuan, X.; Zuo, X.; et al. Effects of hydrogen on the nanomechanical properties of a bulk metallic glass during nanoindentation. *Int. J. Hydrogen Energy* **2017**, *42*, 25436–25445. [CrossRef]
41. Tian, L.; Yang, Y.-Q.; Zhao, X.-A.; Wang, Z.-J.; Xie, D.-G.; Tönnies, D.; Roddatis, V.; Volkert, C.; Shan, Z.-W.; Univerisity of Göttingen, Göttingen, Germany. Unpublished work. 2019.
42. Gibson, J.M.; Treacy, M.M.J.; Voyles, P.M.; Jin, H.C.; Abelson, J.R. Structural disorder induced in hydrogenated amorphous silicon by light soaking. *Appl. Phys. Lett.* **1998**, *73*, 3093–3095. [CrossRef]
43. Voyles, P.M.; Gibson, J.M.; Treacy, M.M.J. Fluctuation microscopy: A probe of atomic correlations in disordered materials. *J. Electron Microsc.* **2000**, *49*, 259–266. [CrossRef] [PubMed]